Virtual Synchronous Machine Control for Asynchronous Grid Connections

Felix Wald *Student Member, IEEE*, Qiucen Tao *Student Member, IEEE*, and Giovanni De Carne *Senior Member, IEEE*

***Abstract*—The reduced amount of large synchronous generators results in the need for fast, flexible, and intelligent power distribution devices to enhance the inertia in the modern power system. This paper proposes a new approach to control an asynchronous low-voltage grid connection, employing a virtual synchronous machine with frequency-based power control. The grid-forming converter, receiving the primary side frequency measurement, varies the fed grid frequency on the secondary side artificially, to interact with frequency-dependent resources. This enables the adjustment of the consumed or generated power in the fed grid without the need for additional communication infrastructure, and thus supports the frequency control of the mains. The performance of the proposed frequency control has been validated through simulation and using a newly developed double Power Hardware-in-the-Loop experimental test setup.**

***Index Terms*—Solid-state transformer, virtual synchronous machine, grid-forming inverter, frequency-based power control, asynchronous grids.**

NOMENCLATURE

Super- and Subscripts

*	Reference
n	Nominal value
0	Initial value (e.g. at $t = 0$)
g	Main grid value
l	LV grid value

Symbols

v_{dc}	DC Voltage
f	Frequency
ω	Angular velocity
θ	Phase angle
K_{pg}	Frequency propagation gain
K_{gen}	Generation gain coefficient
K_{pf}	Active power-to-frequency dependency
K_{scale}	Scaling factor
K_Σ	Sum of gain factors
K_p	Proportional gain
K_i	Integral gain
M	Inertia
J	Moment of inertia
D	Damping
J_{VSM}	Moment of inertia of the VSM
D_{VSM}	Damping of the VSM
P	Active power
P_i	Active power injected/consumed
P_Σ	Total system power
ΔP_m	Conv. generator model power adjustment
ΔP_e	Active power imbalance
ΔP_{scale}	Scaled LV active power adjustment
ΔP_Σ	Summed power deviations
R	Droop coefficient power system model
T_G	Governor time constant
T_{RH}	Reheater time constant
T_{CH}	Main inlet vol. and steam chest time constant
F_{HP}	Fraction of the total turbine power generated
ΔY	Set point for reheat turbine

This work was supported by the Helmholtz Association under the program "Energy System Design" and the Helmholtz Young Investigator Group "Hybrid Networks" (VH-NG-1613).

Felix Wald, Qiucen Tao and Giovanni De Carne are with the Institute of Technical Physics at Karlsruhe Institute of Technology, Karlsruhe, Germany (e-mail: felix.wald@kit.edu).

I. INTRODUCTION

THE evolution of the power system towards a higher penetration of renewable energy resources creates the need to utilize the advantages of power electronic systems. One is the ability to render the power system capable of enduring highly bidirectional power flow and controlling it depending on the system's condition [1]. This control strategy is particularly appealing in combination with the concept of asynchronously-connected grids, shifting its use case from device to grid level. The most prominent technology establishing such an asynchronous connection is the Power Electronic Transformer, also referred to as Solid State Transformer (SST) or Smart Transformer (ST) [2]–[4].

This technology can asynchronously connect two portions of the grid, for example, a low-voltage (LV) grid with the mains. Asynchronous, in this case, means the decoupling of an AC connection between two grids using power electronics (voltage amplitude, frequency and phase do not need synchronization). The only link among them is the active power. The asynchronous connection provides not only voltage transformation and decoupling of the frequency, but also services such as power quality improvement, voltage support or enabling future energy network structures [5]–[12].

Among the proposed services, the support of the medium-voltage (MV) grid by acting on the LV grid has not been studied in detail. Several works mention the support/compensation of voltage and reactive power, but relatively few discuss solutions concerning frequency support [13], [14]. In 2021, Chen et al. investigated, among other scenarios, the impact of SST MV frequency support on systems with high wind penetration. The MV grid support utilizes flexible demand

control, regulating the load power consumption by exploiting the load power to voltage dependency [6]. The results show the positive effect of SSTs on frequency stability, although it should be noted that the results have not been experimentally validated. Following up on these findings, this work will also use the idea of supporting the MV grid by adjusting the active power flow. In the current state of the art, the frequency control of asynchronous grids has been employed for static or slow transients [15], [16]. However, the behavior with dynamic phenomena, such as the primary frequency support of the main power system has only been realized with the use of voltage control [17], [18]. The research on the independent control of the two frequencies to provide primary frequency support to the main system is still incomplete and existing concepts mostly act on passive loads [19]. Additionally, as far as experimental results are concerned this work is one of the few studies providing experimental data interacting with realistic active nodes such as distributed generators and storage units that are frequency dependent (e.g., droop characteristics for batteries or PV), existing research often relies on pure simulations [6], [18]–[24].

This work particularly focuses on a new virtual synchronous machine (VSM) based control method. The VSM control can vary the power consumption of the connected resources to emulate the inertial behavior of a real synchronous machine following significant frequency disturbances. As a consequence, the inertia of the upstream power system can be increased without the need for on-purpose energy storage elements (e.g., batteries). An additional aspect of the work is the use of a simplification of the SST technology. Here, a 2-level LV back-to-back (B2B) converter is deployed. Compared to a SST, the B2B converter can be connected to existing transformer substations or large consumers to enhance functionality and avoid replacing existing systems. In addition, it reaches control decisions autonomously, which provides the flexibility to install it anywhere in the low voltage grid without being restrained to the MV/LV substation.

The novel contributions of this work can be summarized as:

- A frequency-based control, that depending on the mains frequency condition, can control the secondary side frequency, to vary the power consumption and generation of frequency-dependent resources
- Implementation of a Virtual Synchronous Machine algorithm to control the frequency variations in the fed grid, and thus vary the power similar to an equivalent synchronous machine
- Experimental validation of the proposed approach with a double Power Hardware-in-the-Loop setup, where both primary and secondary side of the B2B converter are connected to realistic MV and LV grids

The upcoming sections are structured as follows: section II overviews the general concept of asynchronous connections. In section III its control structure is introduced. Followed by a thorough theoretical system analysis on a simulation basis in section IV, which investigates the impact of the asynchronous connection on a power system. After that, section V offers an in-depth look at the experimental validation of the system in a sophisticated "Power Hardware-in-the-Loop" (PHIL) setup, with a final conclusion drawn in section VI.

II. ASYNCHRONOUS GRID CONCEPT

In recent years many architectures and topologies of power electronic converters have been developed to decouple two connected grids, which can therefore be called asynchronous [9]. The decoupling of two grids not only opens up new possibilities in the control of power systems, but also in the fault protection [16], [25], [26]. To a certain extent, issues in power quality and faults that lead to voltage sags or frequency disturbances will not be propagated to the connected, but AC-decoupled grid [27]. Topologies such as the SST or a B2B converter structure, as shown in Figure 1 can be used to achieve an asynchronous connection.

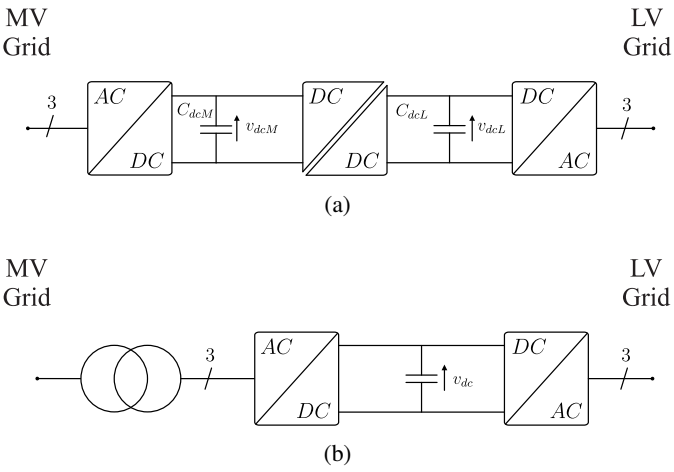

Fig. 1: Power electronic systems that can provide an asynchronous grid connection (a) generic SST topology, (b) B2B converter topology without the DC/DC converter stage.

In the analysis, simulation and experimental validation, a B2B converter system has been used as the power electronic connection to achieve the investigated asynchronous connection with the desired control ability. It has two independent control schemes in place, one for each converter. The primary side is equipped with a common active front-end controller, responsible for keeping the DC-Link at the nominal voltage. This is achieved by employing a cascaded voltage and current controller feeding a PWM firing pulse generator, as illustrated in Figure 2 and previously deployed by [28]–[30]. The secondary side has a more complex multi-layer structure, with a VSM at its core, to which the following sections give detailed insights.

III. FREQUENCY-BASED POWER FLOW CONTROL

This section describes the theory and the implementation behind the proposed frequency-based power flow control for asynchronous grids. In the first part, the implementation of the VSM is described, while the second part introduces the integration of the VSM in frequency-based power flow control. Lastly, the topic of the load and generator dependency on frequency is described to understand what appliances can contribute to the control.

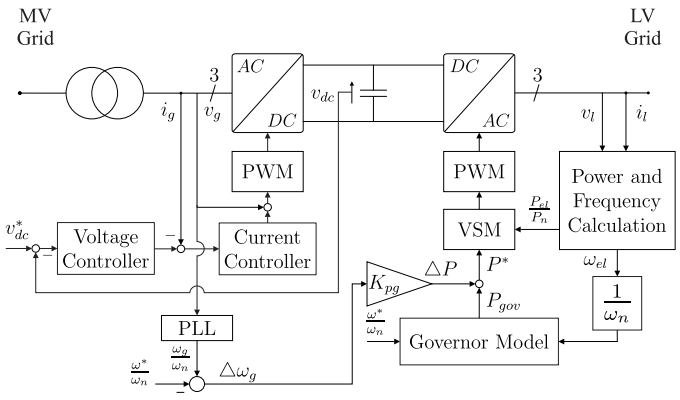

Fig. 2: B2B control structure with the integrated frequency-based power flow control.

A. Virtual Synchronous Machine

On the secondary side of the asynchronous connection, a VSM is deployed to achieve active power flow control. The main goal is to provide frequency support for the MV grid in the inertial and primary control stage of a frequency disturbance. To achieve that, the controller provides the following features to the LV grid:

- Act as a grid forming node - supplying it with high-quality power
- Adjust active power consumption/generation according to the needs of the main grid - without additional communication infrastructure

To achieve a simple and robust controller capable of enduring load steps and frequency variations, the VSM deployed was inspired by the Ise-Lab structure [31].

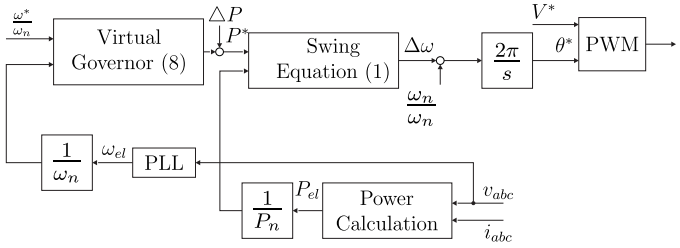

Fig. 3: Implemented VSM control structure after [31].

The general idea of a VSM is to use parts of the mathematical description of a synchronous machine to emulate its behavior. This can be done with different degrees of complexity using n-order models. Complexity, in this case, does not necessarily bring more advantages since a synchronous machine's natural behavior is not always advantageous to a specific application. Therefore, the Ise-Lab structure reduces the synchronous machine model to a second-order model, using mainly the swing equation in (1). The equation describes the interaction of a possible power imbalance between the mechanical power P_m and the electrical power P_{el}, and the change in angular velocity ω depending on the moment of inertia J and damping D. Normally the moment of inertia is related to the physical nature of the rotating part of a synchronous machine. Since the emulation is only a mathematical representation, the moment of inertia can be chosen outside the physically possible boundaries. The nominal angular velocity is represented by ω_n.

$$P^* - P_{el} = J\frac{\dot{\omega}}{\omega_n} + D\frac{\omega}{\omega_n} \tag{1}$$

The VSM control structure is illustrated in Figure 3. In addition to the swing equation, multiple blocks such as a Phase Locked-Loop (PLL), power calculation, and virtual governor model are used to calculate the variables of the VSM. The governor model calculates the power set point for the swing equation to control the frequency to the nominal value of 50 Hz by feeding the frequency from the PLL into a PI controller.

B. Frequency Propagation Concept

The proposed controller, detailed overview seen in Figure 2, uses the frequency deviation Δf of the MV grid paired with a gain K_{pg} to change the active power set point of the VSM. This results in a respective change in the frequency calculated by the VSM, which leads to a change in the active power consumption or generation of the frequency sensible devices in the LV grid. The full concept, signals and power propagation are shown in Figure 4. It can be observed how Δf is used to alter the LV frequency and consequently the active power.

Depending on the load composition, explained in more detail in subsection III-C, the impact of a frequency disturbance on the active power change can be observed.

C. Active Power-to-Frequency Dependency of Low Voltage Grids

The proposed frequency-based power flow controller varies the active power of the LV grid using its frequency-dependent nature. This section discusses the respective active power-to-frequency dependency of commonly connected appliances in LV grids.

In a LV grid, the main appliances are loads, distributed generators and energy storage units. The latter two should actively adjust the active power operating point to support the frequency. According to VDE-AR-N 4105 [32], distributed generators and energy storage systems interfaced to a distribution network should react to frequency deviations of a maximum 51.5 Hz and a minimum 47.5 Hz with a tolerance band of 200 mHz around 50 Hz. As shown in Figure 5, generation units are required to decrease the power generation with a gradient of $0.4\,P_{ref}$ per Hertz for over-frequency. Here, P_{ref} represents the power at 50.2 Hz and is used as a base value for the set point calculation. Meanwhile, storage units should decrease the power with a gradient of $0.4\,P_{Emax}$ per Hertz, where P_{Emax} is the device's maximum power. For under-frequency, power generation units should increase the power with $0.4\,P_{Emax}$ per Hertz when possible, and storage units should increase the power with P_{Emax} per Hertz until the maximum available power is reached. The specified gain of 0.4 p.u. is referred to as K_{gen}, the gain only applies to PV in over-frequency cases, resulting in a power reduction. However, in a general case any generating unit (e.g., a micro-gas turbine), that permits an power upwards regulation, shall

be considered. In under-frequency cases, PV is bound to remain in the same operating point since it is not able to increase its power output, unless it is derated. A detailed list of parameters is available in Table VI. Additionally, the grid standards demand a deadband of ± 0.2 Hz around the nominal frequency of 50 Hz. This avoids over reactions and reduces stress for the connected nodes in cases of a minor, uncritical frequency disturbance [32].

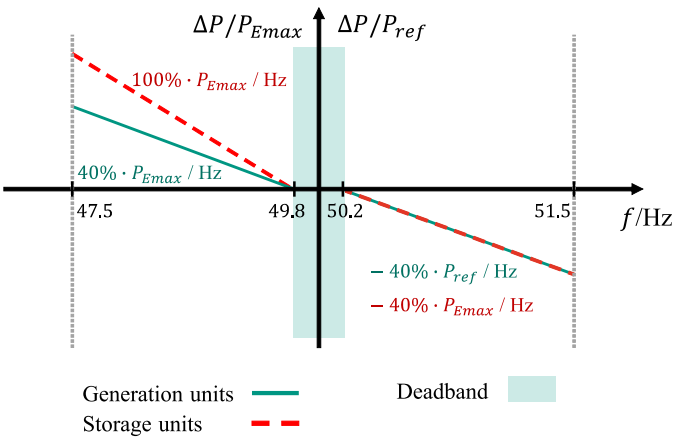

Fig. 5: VDE-AR-N 4105 requirements on active power adjustments at over-frequency and under-frequency for generation units and energy storage units in LV grids [32].

The linear load model is frequently used to describe the active power-to-frequency dependency of loads. It can be expressed as:

$$P = P_0 \cdot \left(1 + K_{pf} \frac{\Delta f}{f_0}\right) \tag{2}$$

where P_0 is the power at f_0. Δf is the difference between the operating frequency and f_0. K_{pf} represents the active power-to-frequency dependency.

In [33], [34] typical values of K_{pf} for individual devices are provided. Depending on the type of the device, the typical value of K_{pf} varies from -1.0 to 5.6. In 1993 the IEEE Task Force on Load Representation for Dynamic Performance compiled a list of typical frequency dependencies for different aggregated loads in North America [35]. The season and heating system have a big impact on the dependency values. The value for residential loads can vary from 0.7 to 1 and between 1.2 and 1.7 for commercial loads. Meanwhile, industrial loads have a K_{pf} value of 2.6. More recent results of industrial loads are provided in [36], [37].

IV. SYSTEM ANALYSIS

The previous section illustrates the feasibility of the active power adjustment based on frequency control. The impact of the power flow change on the main grid has yet to be investigated. Therefore, a comprehensive system analysis is provided in this section, using the developed asynchronous connection integrated into a single machine grid model. This can determine its impact on the grid model at simulation stage, as in [17]. The general combined model shown in Figure 6 is based on a single machine model developed by Kundur et al., it consists of a speed droop block (3), a governor model (4) and a reheat turbine (5) [38].

$$\frac{\Delta P_g}{\Delta \omega} = -\frac{1}{R} \tag{3}$$

$$\frac{\Delta Y}{\Delta P_g} = \frac{1}{1 + sT_G} \tag{4}$$

The ratio between the change in angular velocity $\Delta\omega$ and the change in the power output ΔP_g or valve/gate position is represented by R. The governor model then integrates the power deviation ΔP_g to generate the control signal ΔY, used by the reheat turbine as a set point. The transfer function of the reheat turbine (5) is based on a simplified model, using T_{CH} as the time constant of the main inlet volumes and steam chest, T_{RH} for the time constant of the reheater and F_{HP} as the fraction of the total turbine power generated. It uses the control signal ΔY to achieve a change in the mechanical power output ΔP_m.

$$\frac{\Delta P_m}{\Delta Y} = \frac{1 + sF_{HP}T_{RH}}{(1 + sT_{CH})(1 + sT_{RH})} \tag{5}$$

Since the model resembles the behavior of a single machine, it behaves in a similar fashion as the VSM. A potential power imbalance causes a variation of the angular velocity, in other

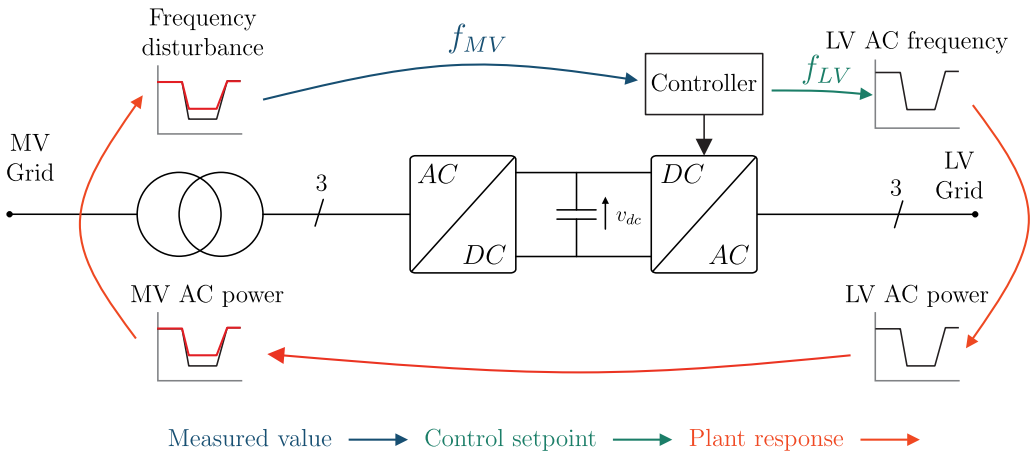

Fig. 4: Overview of the general power flow control concept.

words, a frequency deviation or vice versa. The deviation depends on the power system's inertia M and damping D. Represented by the transfer function:

$$\frac{\Delta\omega}{\Delta P_\Sigma} = \frac{1}{Ms + D} \tag{6}$$

The system analysis focuses on the frequency response to a load/generation change in the main grid. This deviation is then used as the initial event for the asynchronous connection as a supporting device. Applying the per-unit system, can illustrate the impact of asynchronous connections on a larger scale by calculating the amount of fed-back power with respect to the nominal power of the system model. A transfer function of the

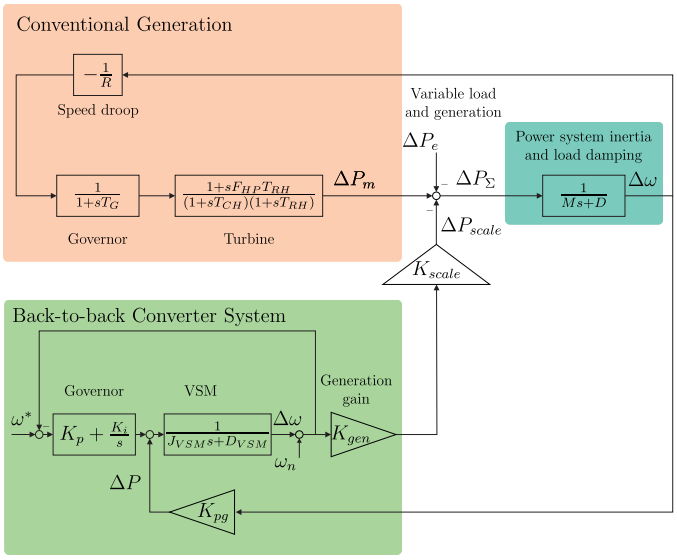

Fig. 6: Single machine grid model combined with a supporting asynchronous connection.

asynchronous connection has been developed for the initial mathematical analysis of the asynchronous connection and its impact on a single machine model. The transfer function consists of a swing equation of the VSM, the virtual governor model and additional gain parameters. Therefore, (1), was converted to the transfer function in (7).

$$\frac{\Delta\omega}{P^*} = \frac{1}{J_{VSM}s + D_{VSM}} \tag{7}$$

The PI controller acting as a virtual governor is represented by the transfer function (8), with K_p as proportional gain, K_i the value for the integral gain. P^* is the summed power set point, using the propagated power imbalance ΔP and the power set point calculated by the virtual governor P_{gov}.

$$\frac{P_{gov}}{\Delta\omega} = K_p + \frac{K_i}{s} \tag{8}$$

For simulation and testing, the LV grid consists of a large share of storage systems and renewable energy resources. Therefore, the K_{pf} value of generation and storage units, illustrated in subsection III-C is used but referred to as K_{gen}. To emulate the effect of multiple or scaled asynchronous connections on the main grid, a scaling factor K_{scale} is used to adjust the amount of the controllable power from the aggregated converter systems. Since all the parameters are calculated in per unit, the scaling factor can set the relation between the sum of LV active power consumption/generation P_i and the total system power P_Σ, as in (9).

$$K_{scale} = \frac{\sum P_i}{P_\Sigma} \tag{9}$$

In short, for a scaling factor of 10%, the total power interfaced with asynchronous connections equals 10% of the total nominal grid power. The two coefficients combined will be referred to as K_Σ:

$$K_\Sigma = K_{scale} K_{gen} \tag{10}$$

The combination of (9) and (10) leads to a second order transfer function of the whole asynchronous connection, shown in (11).

$$\frac{\Delta P_{scale}}{\Delta\omega} = \frac{K_\Sigma(K_p s + K_i)}{J_{VSM}s^2 + D_{VSM}s} \tag{11}$$

The frequency propagation gain factor has been set to $K_{pg} = 40000$, this value results from the fact that the B2B system model is calculated in absolute values whereas the power system model is held in per unit. In this case, $K_{pg} = 40000$ implies a change of $40\,\text{kW}$ for each per-unit of frequency, or $0.8\,\text{kW/Hz}$ in the experimental setup. All parameters used for the system analysis are displayed in Table I. The derived transfer function was then tested in a simulation, using the single machine model as an example power system. With a larger percentage of power provided by the asynchronous connections, the frequency response of the power system has higher inertia and a slightly increased damping. This can be observed in the simulation results shown in Figure 7.

TABLE I: System Analysis Parameter.

Parameter	Value	Parameter	Value
R (p.u.)	0.05	D (p.u.)	1
T_G (s)	0.2	J_{VSM} (p.u.)	0.1
T_{RH} (s)	7	D_{VSM} (p.u.)	1
T_{CH} (s)	0.3	K_{gen} (p.u.)	0.4
F_{HP} (p.u.)	0.3	K_{pg} (W/p.u.)	40000
M (p.u.)	6	K_{Scale} (p.u.)	[0 0.01 0.05 0.1 0.15 0.2]

In Figure 7a, the red line displays the system behavior without any integration of asynchronous connections, the other lines show the impact for the increased share of asynchronous connections, by increasing the parameter $K_{scale} = [0\,\%, 5\,\%, 10\,\%, 15\,\%, 20\,\%]$. It can be seen that, as the total amount of power dispatched by the asynchronous connection increases (Figure 7b), the dispatch of conventionally generated power decreases from the initial moment of the perturbation (Figure 7c). The detailed results are displayed in Table II. The results show that the asynchronous connection can support the main grid during frequency disturbances. E.g. when a $10\,\%$ penetration level is achieved, the nadir is reduced by more than $20\,\%$ compared to the unsupported system and the Rate of Change of Frequency (RoCoF) is, with $0.0547\,\text{Hz/s}$, less than half of the original $0.1176\,\text{Hz/s}$.

It has to be noted that this analysis considers ideal models of the grid components. This means, in contrast to the experimental validation (section V), that neither the non-linearity

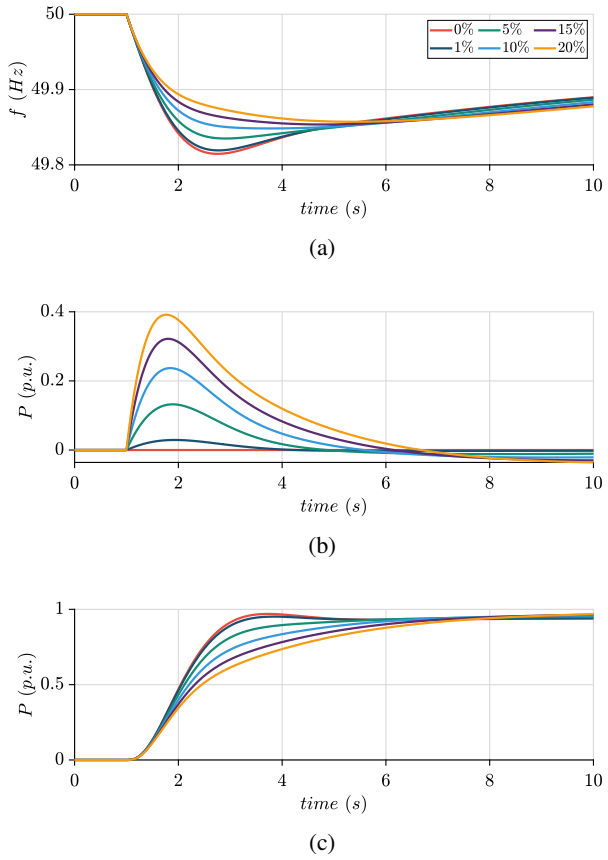

Fig. 7: System response to a load step for increased penetration levels of asynchronous grid connections in a power grid model: (a) resulting frequency of the grid model, (b) total active power dispatched by the asynchronous grids, and (c) by the conventional generator.

TABLE II: System Analysis Results

Feed-in (%)	Nadir (Hz)	RoCoF (Hz/s)
0 %	49.8147	0.1176
1 %	49.8192	0.1020
5 %	49.8350	0.0864
10 %	49.8484	0.0547
15 %	49.8536	0.0387
20 %	49.8572	0.0327

of the droop controller with its mandatory dead-band nor the power limitation of the B2B converter systems are included. However, this analysis shows a clear performance trend of asynchronous grids providing frequency support to increase the system inertia.

V. EXPERIMENTAL EVALUATION

Experimental tests have been performed to validate the performance of the asynchronous grid connection in supporting the MV frequency. The tests were conducted in the PHIL setup in the ”Energy-Lab 2.0” at the Karlsruhe Institute of Technology (KIT), shown in Figure 8.

A. Power Hardware-in-the-Loop Setup

As the hardware under test (HUT), the B2B converter cabinet (red box) is connected to two 200 kVA EGSTON Compiso amplifiers (green boxes), displayed in Figure 8. Each emulates one of the asynchronously connected grids. The primary side emulating the MV grid runs in closed-loop operation as a three-phase voltage source (i.e., voltage-type PHIL algorithm), with an adjustable frequency set point controlled by the single machine model. As explained in the earlier sections, this enables the interaction of the asynchronous connection with a simulated grid. The secondary side consists of a simplified LV grid composed of a passive load, PV, and a battery system. It is also operated in closed-loop, but as a three-phase current source (i.e., current-type PHIL algorithm) [39]. This way, the secondary side acting as a grid-forming entity is connected to an amplifier operating as a three-phase current source. The output voltages on the LV grid side were measured and fed into the distribution grid model. The resulting currents are used as set points for the amplifier.

Figure 8, shows the laboratory setup and a schematic with the devices used for the experimental validation. At the top, the grid models simulated on the real-time simulator are displayed. The models calculate and communicate the set points to the amplifiers. The communication with the amplifiers, seen on the left and right side of the figure, is established by a fiber optic connection using ”small form-factor pluggable” (SFP) transceivers. To close the loop on both sides, the measured values are fed into an IO-Extension Box (purple box), which sends the values to the simulator.

B. Active Power Flow Control

To validate the feasibility of the proposed power flow control and exploit the active power-to-frequency dependency of the LV grid, a simple frequency disturbance on the MV grid is used as a first test case. The results in Figure 9, illustrate the active power adjustment due to a change in the frequency in the main grid at $t = 1\,s$. It is achieved by controlling the LV frequency as explained in subsection III-B.

The green line in Figure 9a shows the frequency step in the main grid, which is amplified and used as a set point for the secondary side controller. Due to the VSM controller, the frequency deviation is damped and brought back to 50 Hz (blue line in Figure 9a). When the frequency is below 49.8 Hz, the power generation of the battery on the LV side increases, resulting in decreased active power consumption of the LV grid. It can be seen that, following the crossing of 49.8 Hz, the active power flow is immediately reduced until the frequency deviation reaches its lowest point (Figure 9b). After which it rises back to the original nominal active power consumption, at $t = 2.84\,s$. The change in the active power depends on the nadir of the frequency deviation in the main grid, the amplification gain of its propagation (k_{pg}), and load behavior, which in this case refers to the droop characteristics. In the tested configuration, the LV frequency deviation is three times bigger than the one in the MV grid, which changes the active power consumption. This proves the capability of the proposed technology and control strategy to change the active

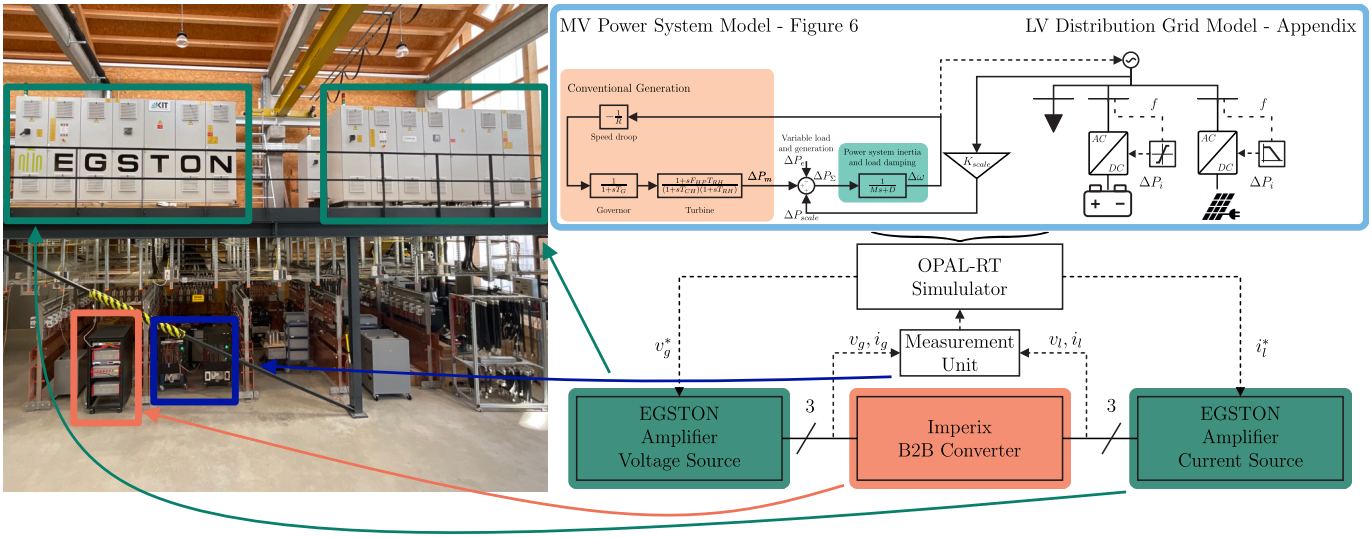

Fig. 8: Power Hardware-in-the-Loop setup to test asynchronously connected grids.

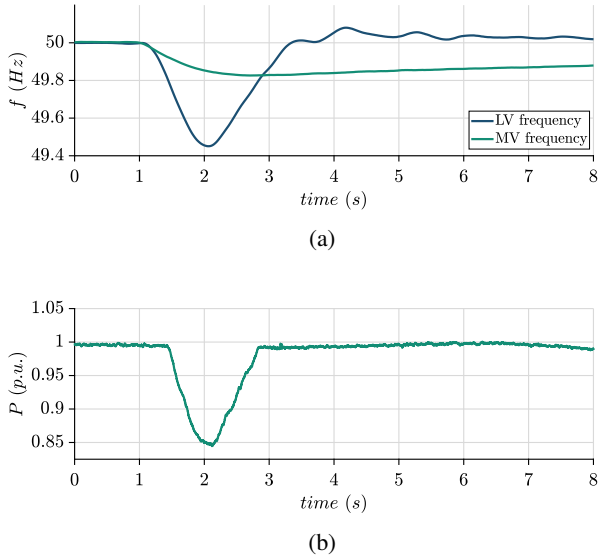

Fig. 9: (a) MV (green) and the propagated LV (blue) frequency; (b) resulting change of power consumption.

power through the frequency and therefore support the MV grid on the primary side.

C. Main Grid Frequency Support

The final validation step shows precisely how the asynchronous connection can support the MV grid and where its limits are. For this, the power adjustment in the asynchronous connection is now fed back to the power system model, previously introduced in section IV. Similar to the investigation made in the simulation, the scaling factor k_{scale} is used to investigate the increased share of asynchronous connections in a power system. In addition to the system analysis on simulation level, the experimental setup, includes the non-linear behavior of loads, generation units and the power limitation of the asynchronous connection. Figure 10,

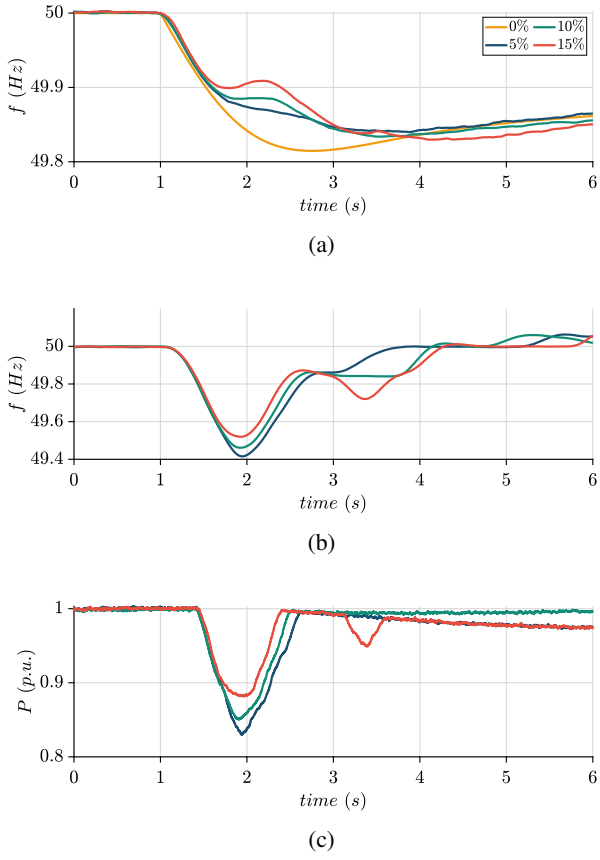

Fig. 10: PHIL test results showing the impact of different feed-in % on the (a) MV grid frequency, (b) LV frequency, and (c) active power dispatched by a single supporting system.

displays the impact of the active power adjustment in the LV grid on the MV frequency. It compares four different degrees of asynchronous connection penetration in the power system. As a benchmark case, the 0 % penetration level is used to describe the system performance without support. Increasing the share of controllable power to 10 % and 15 %, notable

differences can be observed in the frequency behavior, as the nadir decreases ca. 1 mHz per percent. An in-depth look into the results is provided in Table III, showing that the RoCoF is reduced by nearly 50 % for all penetration levels. The nadir of the 10 % and 15 % case is reduced by 11 % and 9 %, while the 5 % case, has a 14 % reduction compared to the unsupported case. The difference between the penetration levels is most likely caused by the additional fluctuation ($t = 2.2\,s$) of the frequency in the 10 % and 15 % case. In the next test case, the

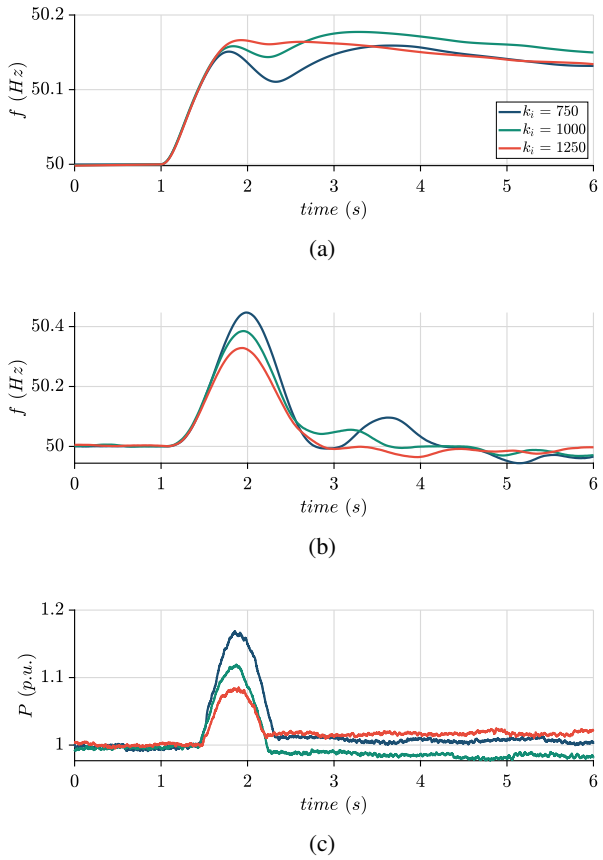

Fig. 11: PHIL test results, for different integrator gains in the governor of the VSM: (a) impact on the MV grid frequency, (b) LV frequency, and (c) active power dispatched by a single supporting system.

impact of the VSM's virtual governor parameter k_i (8) on the LV frequency set point is verified. The resulting frequency and power response are depicted in Figure 11. The lines representing the MV frequency in Figure 11a, show that for an increase of the parameter k_i the frequency response has fewer oscillations. The small dip at around $t = 2.2\,s$ in the red line is only 3 % of its nadir. At the same time reaching the nadir at $t = 1.93\,s$ takes more time, 10 % compared to $k_i = 1000$ and 15 % compared to $k_i = 750$. The oscillations e.g. in case 1 with $k_i = 750$, reflect to the LV side, resulting in a second frequency increase at around $t = 3\,s$. For larger frequency deviations or larger values of k_i, it can lead to a frequency outside the $\pm 0.2\,Hz$ boundary and cause another active power adjustment. Therefore, a good compromise between speed and smooth behavior should be achieved, e.g. $k_i = 1000$, which was used for all the other test cases in this section.

TABLE III: PHIL results - for different penetration levels.

Feed-in (%)	Nadir (Hz)	RoCoF (Hz / s)
0 %	49.8147	0.1176
5 %	49.8399	0.0556
10 %	49.8338	0.0658
15 %	49.8297	0.0542

To account for systems of different inertia caused by the integration of renewable energy resources, the following paragraph discusses test results for frequency support of systems with inertia values of M = [4, 6]. Figure 12, displays frequency and active power flow for the mentioned system with a penetration level of 0 % and 5 %. For an inertia value of $M = 6$ the tests resulted in a reduction of the RoCof by 35 %, but increased the nadir for a slight amount of 8 mHz. For the lower inertia value of $M = 4$, it can be seen that the inherent increase of oscillations tends to be amplified by the support of the asynchronous connection. On the other hand, it comes with the positive effect of decreasing the RoCoF, by nearly 50 % and reducing the nadir by 10 mHz, compared to the unsupported MV frequency response.

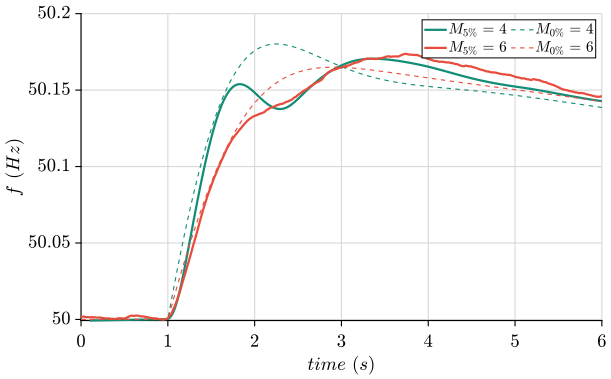

Fig. 12: PHIL test results, displaying the MV frequency for the same test case with 0 % (dashed lines) and 5 % (continuous lines) penetration, under different system inertia (M) conditions.

Thus, it can be concluded that the proposed concept can support the reduction of the RoCoF and limit the nadir in low inertia systems, which can be interpreted as a form of inertia increase. Nevertheless, the impact depends on the conditions of the grid and the amount of connected supporting systems. An increase in oscillations, as seen in the solid green line at $t = 1.8\,s$ in Figure 12, could be avoided by reducing the speed at which the LV side reacts to the frequency perturbation. This is achievable by adjusting the integral gain parameter k_i, as shown in the previous paragraph in Figure 11a.

VI. Conclusion

Due to the increased integration of distributed and renewable power generation, the modern power system is in need for inertia enhancement and flexible power control. As a solution, this paper proposes a frequency-based active power control

TABLE IV: PHIL results - for different system inertia.

Inertia M (p.u.)	Feed-in (%)	Nadir (Hz)	RoCoF (Hz/s)
4	0 %	50.1801	0.1441
4	5 %	50.1705	0.072
6	0 %	50.165	0.08637
6	5 %	50.1737	0.06335

concept for asynchronous grid connections. The frequency support has been achieved by implementing a grid-forming VSM algorithm on the LV side of B2B converter, which modifies the active power consumption/generation of the connected appliances, exploiting the active power-to-frequency dependency in the LV grid. The proposed concept is experimentally validated in a double closed-loop PHIL setup, using a B2B converter to realize the asynchronous grid connection. The measurements show that the proposed control strategy can reduce the RoCoF by up to 50 %, while limiting the resulting nadir during frequency disturbances in the MV grid. The nadir reduction lies in the range of 9 % to 14 % depending on the relative amount of power interfaced through the developed asynchronous connection. All of the aggregated results are subject to the nature of the grid and its condition, it has been shown that the impact of the system inertia can be mitigated, by adjusting the controller speed, while still reducing the RoCoF and nadir. The achieved results show the capability of such an asynchronous connection to provide frequency support and artificial inertia to the mains.

APPENDIX

The LV grid consists of three buses based on values used by the European configuration of the CIGRE LV distribution network benchmark for underground lines. Specific values are displayed in Table V [40].

TABLE V: Primitive impedance matrix $(\Omega\,/\,\mathrm{km})$ [40].

Phase	A	B	C
A	0.287+j0.167	0.121+j0.110	0.125+j0.070
B	0.121+j0.110	0.279+j0.203	0.121+j0.110
C	0.125+j0.070	0.121+j0.110	0.287+j0.167

The components of the LV network are; a dynamic PQ-Load, a Battery Storage System and a PV-System, the last two are equipped with a droop controller. The nominal values during the experimental validation are shown in Table VI.

TABLE VI: Load parameters in the LV distribution network.

Component	P_n	Gain coefficient (p.u.) $f < 49.8Hz$	Gain coefficient (p.u.) $f > 50.2Hz$
B2B - System	8 kW	-	-
PQ-Load	20 kW	-	-
Battery	8 kW	0.4	1.0
PV	4 kW	0	0.4

REFERENCES

[1] G. De Carne, G. Buticchi, M. Liserre, and C. Vournas, "Load Control Using Sensitivity Identification by Means of Smart Transformer," *IEEE Transactions on Smart Grid*, vol. 9, no. 4, pp. 2606–2615, Jan. 2018.

[2] W. McMurray, "Power converter circuits having a high frequency link," US Patent US3 517 300A, Jun., 1970.

[3] X. She, A. Q. Huang, and R. Burgos, "Review of Solid-State Transformer Technologies and Their Application in Power Distribution Systems," *IEEE Journal of Emerging and Selected Topics in Power Electronics*, vol. 1, no. 3, pp. 186–198, Jan. 2013.

[4] M. Liserre, G. Buticchi, M. Andresen, G. De Carne, L. F. Costa, and Z.-X. Zou, "The Smart Transformer: Impact on the Electric Grid and Technology Challenges," *IEEE Industrial Electronics Magazine*, vol. 10, no. 2, pp. 46–58, Jun. 2016.

[5] R. Zhu, Z. Zou, and M. Liserre, "High Power Quality Voltage Control of Smart Transformer-Fed Distribution Grid," in *IECON 2018 - 44th Annual Conference of the IEEE Industrial Electronics Society*, Jan. 2018, pp. 5547–5552.

[6] J. Chen, M. Liu, G. De Carne, R. Zhu, M. Liserre, F. Milano, and T. O'Donnell, "Impact of smart transformer voltage and frequency support in a high renewable penetration system," *Electric Power Systems Research*, vol. 190, Jan. 2021.

[7] J. E. Huber and J. W. Kolar, "Applicability of Solid-State Transformers in Today's and Future Distribution Grids," *IEEE Transactions on Smart Grid*, vol. 10, no. 1, pp. 317–326, Jan. 2019.

[8] R. Zhu, G. Buticchi, and M. Liserre, "Investigation on Common-Mode Voltage Suppression in Smart Transformer-Fed Distributed Hybrid Grids," *IEEE Transactions on Power Electronics*, vol. 33, no. 10, pp. 8438–8448, Jan. 2018.

[9] L. Ferreira Costa, G. De Carne, G. Buticchi, and M. Liserre, "The Smart Transformer: A solid-state transformer tailored to provide ancillary services to the distribution grid," *IEEE Power Electronics Magazine*, vol. 4, no. 2, pp. 56–67, Jan. 2017.

[10] S. Bifaretti, P. Zanchetta, A. Watson, L. Tarisciotti, and J. C. Clare, "Advanced Power Electronic Conversion and Control System for Universal and Flexible Power Management," *IEEE Transactions on Smart Grid*, vol. 2, no. 2, pp. 231–243, Jun. 2011.

[11] A. Q. Huang, M. L. Crow, G. T. Heydt, J. P. Zheng, and S. J. Dale, "The Future Renewable Electric Energy Delivery and Management (FREEDM) System: The Energy Internet," *Proceedings of the IEEE*, vol. 99, no. 1, pp. 133–148, Jan. 2011.

[12] C. Kumar and M. Liserre, "A new prospective of smart transformer application: Dual microgrid (DMG) operation," in *IECON 2015 - 41st Annual Conference of the IEEE Industrial Electronics Society*, Nov. 2015, pp. 004 482–004 487.

[13] D. Shah and M. L. Crow, "Online Volt-Var Control for Distribution Systems With Solid-State Transformers," *IEEE Transactions on Power Delivery*, vol. 31, no. 1, pp. 343–350, Feb. 2016.

[14] C. Kumar and M. Liserre, "Operation and control of smart transformer for improving performance of medium voltage power distribution system," in *2015 IEEE 6th International Symposium on Power Electronics for Distributed Generation Systems (PEDG)*, Jun. 2015, pp. 1–6.

[15] G. De Carne, G. Buticchi, Z. Zou, and M. Liserre, "Reverse Power Flow Control in a ST-Fed Distribution Grid," *IEEE Transactions on Smart Grid*, vol. 9, no. 4, pp. 3811–3819, Jan. 2018.

[16] G. De Carne, Z. Zou, G. Buticchi, M. Liserre, and C. Vournas, "Overload Control in Smart Transformer-Fed Grid," *Applied Sciences*, vol. 7, no. 2, p. 208, Jan. 2017.

[17] G. De Carne, G. Buticchi, M. Liserre, and C. Vournas, "Real-Time Primary Frequency Regulation Using Load Power Control by Smart Transformers," *IEEE Transactions on Smart Grid*, vol. 10, no. 5, pp. 5630–5639, Jan. 2019.

[18] J. Chen, C. O'Loughlin, and T. O'Donnell, "Dynamic demand minimization using a smart transformer," in *IECON 2017 - 43rd Annual Conference of the IEEE Industrial Electronics Society*, 2017, pp. 4253–4259.

[19] Q. Tao, J. Geis-Schroer, F. Wald, M. Courcelle, M. Langwasser, T. Leibfried, M. Liserre, and G. De Carne, "The potential of frequency-based power control in distribution grids," in *2022 IEEE 13th International Symposium on Power Electronics for Distributed Generation Systems (PEDG)*, 2022, pp. 1–6.

[20] O. Gomis-Bellmunt, S. D. Tavakoli, V. A. Lacerda, and E. Prieto-Araujo, "Grid-forming loads: Can the loads be in charge of forming the grid in modern power systems?" *IEEE Transactions on Smart Grid*, pp. 1–1, 2022.

[21] M. G. Dozein, A. Jalali, and P. Mancarella, "Fast frequency response from utility-scale hydrogen electrolyzers," *IEEE Transactions on Sustainable Energy*, vol. 12, no. 3, pp. 1707–1717, 2021.

[22] D. Ramasubramanian, "Importance of considering plant ramp rate limits for frequency control in zero inertia power systems," in *2021 IEEE Green Technologies Conference (GreenTech)*, 2021, pp. 320–322.

[23] P. Babahajiani, Q. Shafiee, and H. Bevrani, "Intelligent demand response contribution in frequency control of multi-area power systems," *IEEE Transactions on Smart Grid*, vol. 9, no. 2, pp. 1282–1291, 2018.

[24] S. Weckx, R. D'Hulst, and J. Driesen, "Primary and Secondary Frequency Support by a Multi-Agent Demand Control System," *IEEE Transactions on Power Systems*, vol. 30, no. 3, pp. 1394–1404, May 2015.

[25] J. Rodrigues, C. Moreira, and J. P. Lopes, "Fault-Ride-Through Approach for Grid-Tied Smart Transformers without Local Energy Storage," *Energies*, vol. 14, no. 18, p. 5622, Jan. 2021.

[26] G. De Carne, G. Buticchi, M. Liserre, and C. Vournas, "Frequency-Based Overload Control of Smart Transformers," in *2015 IEEE Eindhoven PowerTech*. IEEE, Jan. 2015, pp. 1–5.

[27] X. She, X. Yu, F. Wang, and A. Q. Huang, "Design and Demonstration of a 3.6-kV–120-V/10-kVA Solid-State Transformer for Smart Grid Application," *IEEE Transactions on Power Electronics*, vol. 29, no. 8, pp. 3982–3996, Jan. 2014.

[28] A. Yazdani and R. Iravani, *Voltage-sourced converters in power systems: Modeling, control, and applications*. John Wiley & Sons, Jan. 2010.

[29] R. Teodorescu, M. Liserre, and P. Rodríguez, Eds., *Grid converters for photovoltaic and wind power systems*. John Wiley & Sons, Jan. 2011.

[30] D. Gross, E. Sanchez-Sanchez, E. Prieto-Araujo, and O. Gomis-Bellmunt, "Dual-port grid-forming control of mmcs and its applications to grids of grids," *IEEE Transactions on Power Delivery*, pp. 1–1, 2022.

[31] K. Sakimoto, Y. Miura, and T. Ise, "Stabilization of a power system with a distributed generator by a Virtual Synchronous Generator function," in *8th International Conference on Power Electronics - ECCE Asia*, Jan. 2011, pp. 1498–1505.

[32] "Power Generating Plants in the Low Voltage Network - Erzeugungsanlagen am Niederspannungsnetz (VDE-AR-N 4105)." [Online]. Available: https://www.vde.com/vde-ar-n-4105-2018

[33] C. W. Taylor, *Power System Voltage Stability*. McGraw Hill, 1994.

[34] C. Concordia and S. Ihara, "Load Representation in Power System Stability Studies," *IEEE Transactions on Power Apparatus and Systems*, no. 4, pp. 969–977, Apr. 1982.

[35] W. W. Price, "Load representation for dynamic performance analysis (of power systems)," *IEEE Transactions on Power Systems*, vol. 8, no. 2, pp. 472–482, May 1993.

[36] Y. Li, H.-D. Chiang, B.-K. Choi, Y.-T. Chen, D.-H. Huang, and M. G. Lauby, "Representative static load models for transient stability analysis: development and examination," *IET Generation, Transmission & Distribution*, vol. 1, no. 3, pp. 422–431, May 2007.

[37] L. M. Korunovic, J. V. Milanovic, S. Z. Djokic, K. Yamashita, S. M. Villanueva, and S. Sterpu, "Recommended Parameter Values and Ranges of Most Frequently Used Static Load Models," *IEEE Transactions on Power Systems*, vol. 33, no. 6, pp. 5923–5934, Jan. 2018.

[38] N. J. Balu, M. G. Lauby, and P. S. Kundur, Eds., *Power system stability and control*. McGraw Hill, Jan. 1994.

[39] G. De Carne, G. Buticchi, and M. Liserre, "Current-type Power Hardware in the Loop (PHIL) evaluation for smart transformer application," in *2018 IEEE International Conference on Industrial Electronics for Sustainable Energy Systems (IESES)*, Jan. 2018, pp. 529–533.

[40] K. Strunz, E. Abbasi, R. Fletcher, N. Hatziargyriou, R. Iravani, and G. Joos, "TF C6.04.02 : TB 575 – Benchmark Systems for Network Integration of Renewable and Distributed Energy Resources," CIGRE, Tech. Rep., Apr. 2014.

Felix Wald (S'20) received his bachelor's degree from Berlin University of Applied Sciences in 2019 and his master's degree from the Karlsruhe Institute of Technology in 2021, in electrical engineering. Since February 2021 he is working towards his Ph.D. degree as part of the "Real Time System Integration" group and "Power Hardware-in-the-Loop" lab at the Institute for Technical Physics at the Karlsruhe Institute of Technology, Karlsruhe, Germany. He is an active member of the IEEE PES Taskforce on Solid State Transformer integration in distribution grids and his research interests include Power Hardware-in-the-Loop validation and the technical and economic investigation of power electronic transformers.

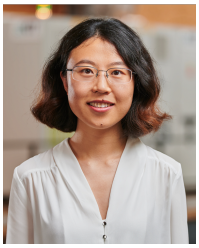

Qiucen Tao (S'22) received her bachelor's degree from Southeast University, China, in 2017, and her master's degree from the Karlsruhe Institute of Technology, Germany, in 2021, in electrical engineering. She is currently working towards her Ph.D. degree as part of the "Real Time System Integration" Group and "Power Hardware In the Loop Lab" at the Karlsruhe Institute of Technology. She is currently working on the sensitivity identification and control of distribution networks, and the Power Hardware-in-the-Loop implementation of them.

Giovanni De Carne (S'14, M'17, SM'21) received the B.Sc. and M.Sc. degrees in electrical engineering from the Polytechnic University of Bari, Italy,in 2011 and 2013, respectively, and the Ph.D. degree from the Chair of Power Electronics, Kiel University, Germany, in 2018. He was post-doctoral fellow at Kiel University working on HVdc control and services until 2019. He is currently Tenure-Track professor at the Institute for Technical Physics at the Karlsruhe Institute of Technology, Karlsruhe, Germany, where he leads the "Real Time System Integration" Group and he is the head of the "Power Hardware In the Loop Lab". In 2020, Dr.-Ing. De Carne has been awarded with the Helmholtz "Young Investigator Group" for the project "Hybrid Networks: a multi-modal design for the future energy system". He has authored/coauthored more than 80 peer-reviewed scientific papers. His research interests includes power electronics integration in power systems, solid state transformers, real time modelling, and power hardware in the loop. He is an Associate Editor of the IEEE Industrial Electronics Magazine and IEEE Open Journal of Power Electronics. He is the chairman of the IEEE PES Task Force on Solid State Transformer integration in distribution grids.